One Earth

Article

Impacts of enhanced new-particle growth events above urban roughness sublayer on cloud condensation nuclei

Graphical abstract

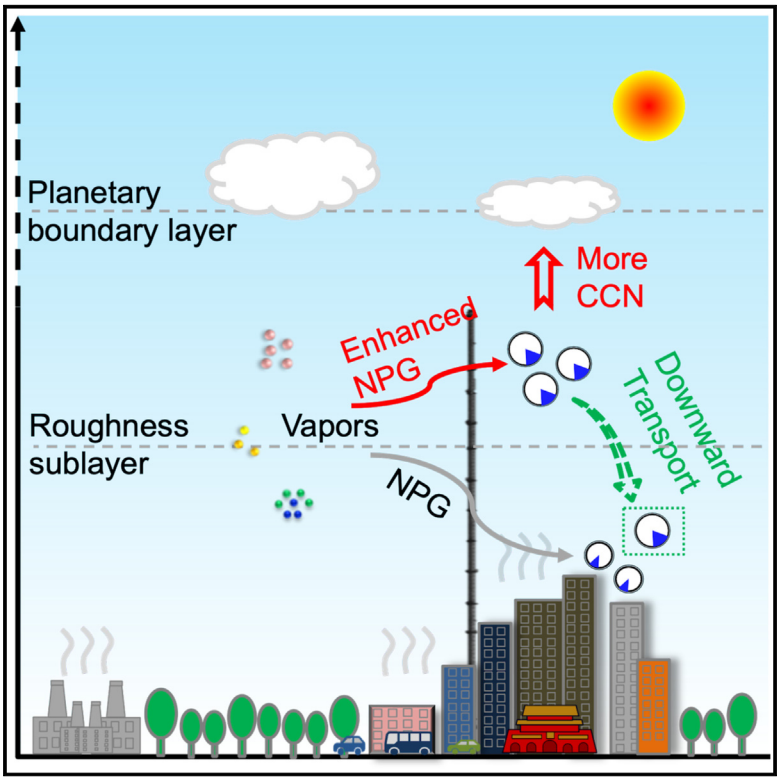

Highlights

- New-particle formation and growth (NPG) aloft is enhanced in the city
- Urban NPG events detected on the ground could originate at higher altitudes
- Enhanced particle growth at higher altitude is associated with higher RH aloft
- The enhancements of cloud condensation nuclei aloft could be up to 20%

Authors

Wei Du, Jian Zhao, Lubna Dada, ..., Veli-Matti Kerminen, Markku Kulmala, Yele Sun

Correspondence

wei.du@helsinki.fi (W.D.), sunyele@mail.iap.ac.cn (Y.S.)

In brief

Why are new-particle formation and growth (NPG) events frequently observed in the urban environment and what are their climate effects? By analyzing aerosol processes at different heights in urban Beijing, this study reveals that NPG is stronger at higher altitudes, leading to increased CCN concentrations aloft. These findings suggest that urban NPG may have a larger impact on climate than previously understood, especially in shaping low-level clouds and altering local climate dynamics.

Du et al., 2025, One Earth *8*, 101169
January 17, 2025
https://doi.org/10.1016/j.oneear.2024.12.005

CellPress

One Earth

CellPress
OPEN ACCESS

Article

Impacts of enhanced new-particle growth events above urban roughness sublayer on cloud condensation nuclei

Wei Du,[1,2,12,*] Jian Zhao,[2] Lubna Dada,[2,3] Weiqi Xu,[1] Yuying Wang,[4] Yu Shi,[1] Xueshun Chen,[1] Tom V. Kokkonen,[2] Jing Cai,[4] Yingjie Zhang,[5] Qingqing Wang,[1] Runlong Cai,[2] Qiaozhi Zha,[6] Libo Zhou,[1] Zhanqing Li,[7] Fangqun Yu,[8] Pingqing Fu,[9] Fei Hu,[1] Zifa Wang,[1] Douglas R. Worsnop,[10] Federico Bianchi,[2] Veli-Matti Kerminen,[2] Markku Kulmala,[2,6,11] and Yele Sun[1,*]

[1]State Key Laboratory of Atmospheric Boundary Layer Physics and Atmospheric Chemistry, Institute of Atmospheric Physics, Chinese Academy of Sciences, Beijing 100029, China
[2]Institute for Atmospheric and Earth System Research / Physics, Faculty of Science, University of Helsinki, Helsinki 00014, Finland
[3]Laboratory of Atmospheric Chemistry, Paul Scherrer Institute, 5232 Villigen, Switzerland
[4]School of Atmospheric Physics, Nanjing University of Information Science and Technology, Nanjing 210044, China
[5]School of Ecology and Nature Conservation, Beijing Forestry University, Beijing 100083, China
[6]Joint International Research Laboratory of Atmospheric and Earth System Sciences, School of Atmospheric Sciences, Nanjing University, Nanjing 210023, China
[7]Earth System Science Interdisciplinary Center and Department of Atmospheric and Oceanic Science, University of Maryland, College Park, MD, USA
[8]Atmospheric Sciences Research Center, State University of New York at Albany, 251 Fuller Road, Albany, NY 12203, USA
[9]Institute of Surface-Earth System Science, Tianjin University, Tianjin 300072, China
[10]Aerodyne Research, Inc., Billerica, MA 01821, USA
[11]Aerosol and Haze Laboratory, Beijing Advanced Innovation Center for Soft Matter Science and Engineering, Beijing University of Chemical Technology, Beijing 100029, China
[12]Lead contact
*Correspondence: wei.du@helsinki.fi (W.D.), sunyele@mail.iap.ac.cn (Y.S.)
https://doi.org/10.1016/j.oneear.2024.12.005

SCIENCE FOR SOCIETY Aerosols, which are fine particles suspended in the atmosphere, can have large impacts on local weather and climate by increasing cloud condensation nuclei and altering how much solar energy is absorbed or reflected by the atmosphere. In cities, the complex sources of atmospheric pollutants, combined with complicated urban atmosphere mixing properties, make it challenging to understand and predict urban aerosol particle formation and weather/climate implications. In this research, we observed new-particle formation at different urban altitudes in Beijing, and found that new-particle formation—and their potential for increasing cloud condensation nuclei—was higher at greater altitudes. The study offers valuable insights for better predicting how urban aerosols contribute to climate change and informing mitigation strategies.

SUMMARY

New-particle formation (NPF) events are frequently observed in urban environments, yet their occurrence and climate effects are still in question. We analyzed the physical and chemical processes during the new-particle growth (NPG) at the ground and 260 m based on measurements on the 325-m tower in the megacity of Beijing, China. Our results provide evidence for stronger NPG aloft in city, mainly due to the higher production of sulfuric acid aloft, and the downwards transport of newly formed particles from the upper atmospheric boundary layer. The particle growth aloft is promoted by the higher relative humidity, facilitating gas-to-particle partitioning, especially of nitrate. Therefore, higher particle concentrations accompanied by stronger hygroscopicity lead to >20% higher NPG-induced cloud condensation nuclei aloft, demonstrating the importance of vertical differences in NPF for a better understanding of the climate effect in urban areas.

Please cite this article in press as: Du et al., Impacts of enhanced new-particle growth events above urban roughness sublayer on cloud condensation nuclei, One Earth (2024), https://doi.org/10.1016/j.oneear.2024.12.005

INTRODUCTION

New-particle formation (NPF) is one of the key processes determining the dynamics of atmospheric aerosols.[1] Identified by high number concentrations of nucleation-mode particles, NPF events have been identified as a five-step process: (1) the formation of low-volatile vapors, (2) clustering, (3) nucleation, (4) the activation of clusters with a second group of vapors, and (5) the subsequent growth process.[2] As a result of the competition between condensable vapor sources and sinks, NPF depends on boundary-layer dynamics and meteorological variables such as the temperature (T) and relative humidity (RH).[3–10] This makes NPF a complex process varying among locations and seasons.[11–15] These newly formed particles can grow to large enough sizes where they can act as cloud condensation nuclei (CCN) affecting cloud properties and the Earth's radiative balance.[16–18] In addition, the continuous growth of newly formed particles in the atmosphere can contribute to haze formation in urban areas.[19–21] The significant implications for global climate and human health[22] make understanding NPF important.

While NPF is identified as one of the most important sources of atmospheric aerosols and CCN, a quantitative estimation of its contribution has a considerable uncertainty.[17,23,24] Current models tend to underestimate the observed CCN concentrations with the largest errors in urban areas mainly due to the effect of urban NPF.[25,26] Additionally, it remains challenging to accurately associate CCN to their source, whether from NPF or primary aerosol particles, especially in urban environments.[15] One of the possible solutions is to conduct real-time size-resolved measurements above the roughness sublayer, where primary emissions are relatively limited. In addition, NPF events observed at the ground level might have started aloft,[27–29] while it has not been directly proved in urban environments.

In this study, we performed simultaneous measurements of particle number size distributions (PNSDs) and chemical compositions at the ground and at 260 m (above the roughness sublayer; see details in experimental design and Note S1), in urban Beijing. By comparing the new-particle growth (NPG) process larger than 20 nm at the two heights, we provide the first observational evidence that NPG was enhanced above the roughness sublayer in urban areas. The enhanced NPG aloft was found to be associated with more readily available sulfuric acid (H_2SO_4), or/and downdraft transport of newly formed particles from the upper atmospheric boundary layer. We then analyzed the particle chemical processes during the NPG events at both heights. The results highlighted the potential contribution of nitrate to particle growth aloft. The enhanced NPG led to higher particle number concentrations accompanied by stronger hygroscopicity aloft, resulting in more particles that could be activated as CCN above the urban roughness sublayer.

RESULTS AND DISCUSSION

Enhanced NPG at 260 m

During our observation, typical NPG events (described in Methods) were observed on 40% of the days at both heights (Figure S1; Table S1). In general, the average PNSDs between 9:00 and 18:00 on NPG days were similar at both heights, characterized by bimodal size distributions peaking at ~35 and ~110 nm, respectively (Figure 1A). The number concentrations of particles smaller than 40 nm at 260 m were higher than those at the ground ($Ratio_{260\ m/ground}$>1). On the contrary, the average PNSDs showed generally higher concentration at the ground level during non-event days (Figure 1B), consistent with higher local emissions near the urban surface.[30–32] The diurnal patterns of PNSD and the formation rate of 20-nm particles (J_{20}) at 260 m and ground level during NPG days are illustrated in Figure 1C. Typical PNSD evolutions of "banana" shapes were observed at both heights after 10:00, while the burst of nucleation-mode particles at 260 m could be detected at 9:00 with PNSD showing an extra nucleation mode peaking under 20 nm (Figure S2). In fact, the formation rate of 20-nm particles at 260 m ($J_{20\ 260m}$) increased by a factor of 10 from 0.1 cm^{-3} s^{-1} at 6:30 to 1.0 cm^{-3} s^{-1} at 11:30, whereas the increase of J_{20} at the ground ($J_{20\ ground}$) started 2 h later and this increase was only a factor of 4, from 0.2 cm^{-3} s^{-1} at 8:30 to 0.8 cm^{-3} s^{-1} at 11:30 (Figure 1C). $J_{20\ 260m}/J_{20\ ground}$ was generally higher than 1 during the growth period. As a result, the ratio of particle number concentration between two heights ($Ratio_{260\ m/ground}$) was larger than 1 during 9:00–17:00. These results suggested enhanced NPG at 260 m.

Since $Ratio_{260\ m/ground}$ higher than 1 was more significant for particles smaller than 40 nm during NPG events, we further divided particles into three size ranges: D_p = 20–40 nm, D_p = 40–100 nm, and D_p = 100–550 nm. The number and mass concentrations of particles in a given size range were denoted as N, and M with D_p ranges as subscripts. During NPG events, $N_{20–40}$ at 260 m increased from 990 cm^{-3} at 6:30 to 6,595 cm^{-3} at 12:30 (a factor of ~7), while it increased from 1,603 cm^{-3} at 8:30 to 6,106 cm^{-3} at 12:30 near the ground (a factor of ~4) (Figure 1D). $N_{40–100}$ showed a similar diurnal evolution to $N_{20–40}$, which was characterized by two high peaks at the ground level but only one peak at 260 m. Driven by particle growth, the noon peak of $N_{40–100}$ at both heights was 1 h later than that of $N_{20–40}$. The diurnal cycle of $N_{100–550}$ was relatively stable at 260 m, while it had a higher number concentration during night-time at the ground level caused by the suppressed vertical mixing of local emissions. $Ratio_{260\ m/ground}$ also showed a significant diurnal variation. In detail, the $Ratio_{260\ m/ground}$ of $N_{20–40}$ and $N_{40–100}$ increased from ~0.6 to ~1.2 and from ~0.8 to ~1.1, respectively, before noon. Such pronounced evolutions cannot be solely explained by the evolution of boundary-layer height and enhanced vertical transport, since otherwise a similar behavior would be observed on non-event days. However, on non-event days, $N_{20–40}$ and $N_{40–100}$, showing two peaks associated with local emissions, had much lower concentrations during the noon peak at both heights (Figure S3). And the $Ratio_{260\ m/ground}$ of $N_{20–40}$ and $N_{40–100}$ was always lower than 0.8 before noon on non-event days, which was consistent with the previous studies showing that the primary particles aloft were generally lower than that near ground during daytime in Beijing.[32,33] In addition, based on the Nested Air Quality Prediction Modeling System with an Advanced Particle Microphysics (NAQPMS + APM, Note S2) model, $N_{20–40}$ and $N_{40–100}$ from primary emissions were lower at 260 m than the ground level during daytime on the NPG-event days (Figure S4). All these results suggested that there was a stronger source of small-size particles at 260 m associated with the growth of newly formed particles (i.e., NPG).

Please cite this article in press as: Du et al., Impacts of enhanced new-particle growth events above urban roughness sublayer on cloud condensation nuclei, One Earth (2024), https://doi.org/10.1016/j.oneear.2024.12.005

CellPress
OPEN ACCESS

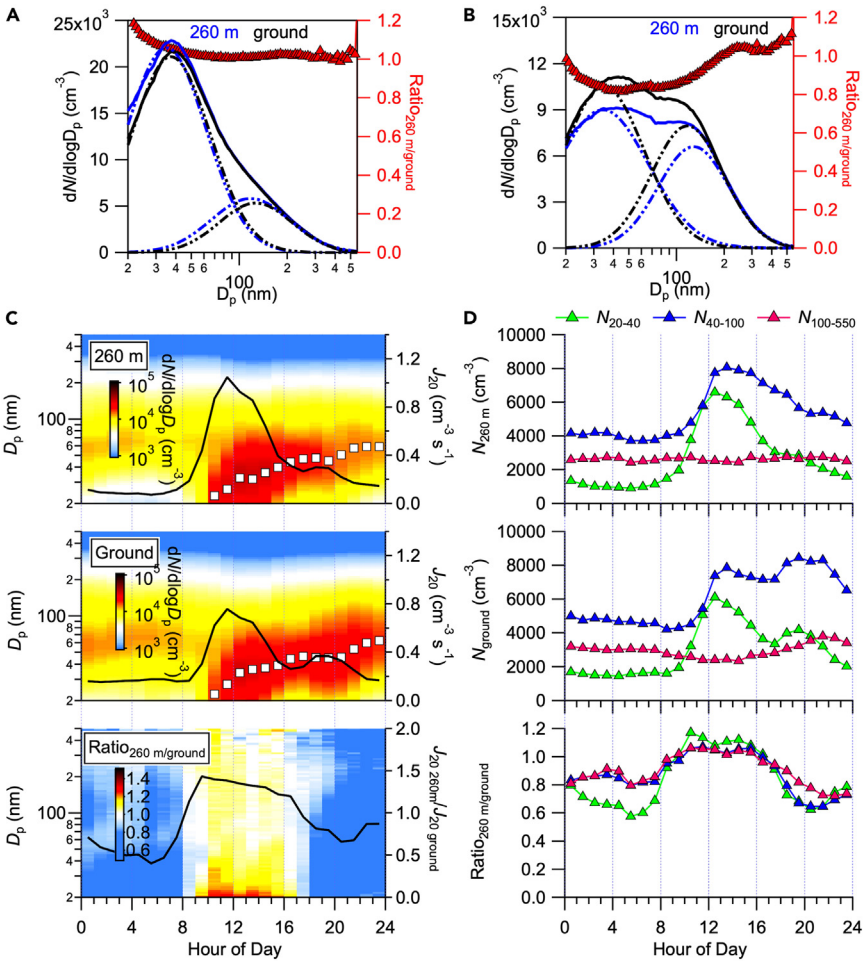

Figure 1. Enhanced NPG events aloft

(A and B) The average particle number size distribution at 260 m (blue) and ground level (black), and the ratios (red) between two heights during (A) new-particle growth (NPG) period, and (B) non-NPG period between 9:00 and 18:00. The dotted lines show bimodal size distributions using log-normal fitting.

(C and D) The average diurnal patterns of (C) particle number size distribution and (D) number concentration (N) in different size ranges (20–40, 40–100, and 100–550 nm) at 260 m, at the ground level, and their ratios between two heights during NPG days, respectively. Black lines in (C) show the formation rate of 20 nm particles (J_{20}) and the ratio between two heights. White squares in (C) are the mean diameters.

We then analyzed each case in detail (Table S1). Time differences were generally observed between the start time of NPG (t_{start}) at 260 m and ground (Δt_{start}), suggesting that nucleation-mode particles were always detected at 260 m first. This can be explained either by an earlier NPF at 260 m and/or stronger growth. In fact, particle growth rate (GR) during the whole NPG period (GR_{all}) was in most cases (60%) higher at 260 m compared to ground level, varying from 2.3 to 9.5 nm h^{-1} at 260 m and from 2.1 to 7.8 nm h^{-1} at the ground. Similarly, J_{20} was always higher at 260 m during NPG events. The peak value of J_{20} ($J_{20\ max}$) at 260 m was >20% higher than that at the ground in most cases (70%). Although, given the instrument cutoff limitation, we cannot accurately determine the start time of each NPF event, our results are a sufficient indication of the enhanced NPG at 260 m compared to ground level. As a result, more particles larger than 20 nm from NPG were expected at 260 m. Since N_{20-40} during NPG days was ~2 times higher than that during non-event days (Figures 1 and S3) at both heights, N_{20-40} on NPG days was suspected to be dominated by newly formed particles. Thus, the ratio of maximum N_{20-40} ($N_{20-40\ max}$) during growth periods between two heights could be used to represent the enhancement factor of NPG at 260 m (Figure S5A). $N_{20-40\ max}$ varied from 5,655 to 16,059 cm^{-3} at the ground level, and from 6,502 to 21,165 cm^{-3} at 260 m. Correspondingly, $Ratio_{260\ m/ground}$ of $N_{20-40\ max}$ was generally higher than 1.0 except for 25 June, on which $Ratio_{260\ m/ground}$ was slightly lower than 1.0 (12,292 cm^{-3} at 260 m vs. 12,650 cm^{-3} at the ground). However, this should not be interpreted as NPG at 260 m not being as strong as that at the ground level, since a much lower ratio during non-event day ($Ratio_{260\ m/ground} < 0.8$) was observed associated with local emissions near ground. In fact, on 25 June, $J_{20\ max}$ was 39.0% higher at 260 m than the ground, associated with a larger GR_{all} (9.5 nm h^{-1} at 260 m vs. 7.3 nm h^{-1} at the ground).

Roles of meteorology and chemistry

An important question is why NPG events were enhanced at 260 m. We found that T might play a minor role, while higher RH aloft was the driving factor behind the enhanced particle growth (Figure 2). Lower T could promote the nucleation process,[34] and hence a negative correlation was obtained between J_{20} and T under similar O_3 concentrations at both heights (Figure S6A). T at 260 m was 24.7°C ± 4.2°C (15.7°C–34.6°C) on average, which was 2.4°C lower than the ground level value of 27.1°C ± 4.4°C (18.3°C–37.8°C) on NPG-event days (Figure S5). However, no strong correlation between $J_{20\ 260m}/J_{20\ ground}$ and temperature differences was observed (Figure S6B), indicating that T was not the driving factor behind the enhancement of J_{20} aloft. One of the possible reasons could be that the temperature difference was not large enough to play a significant role. Although high RH was found to suppress the initial process of NPF in field campaigns,[35,36] as it is associated with the presence of clouds that can limit the photochemical process,[37] recent studies found that high RH benefits particle growth by promoting the vapor condensation and heterogeneous reactions.[20,34] Here, positive correlations between GR_{all} and RH were observed at both heights within certain T ($20 < T < 30$°C, $r = 0.93$) (Figure 2A). NPG on 2 June is an exception, which had relatively low J_{20} and GRs at both heights coupled with the highest RH and lowest T in these NPF days. Note that 2 June was a cloudy day, leading

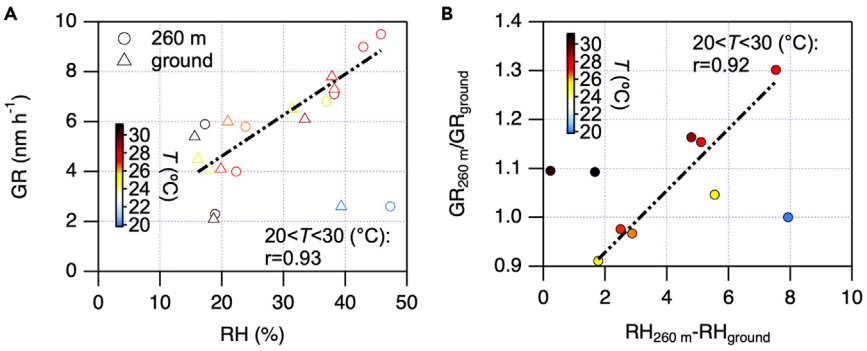

Figure 2. The role of RH in enhanced NPG events aloft

(A) The dependence of GRs on RH colored by temperature at 260 m (circles) and the ground (triangles).

(B) The ratios of GRs between the two heights versus differences in RH between the two heights colored by temperature at 260 m. *T* is temperature, RH is relative humidity, and GR is the GR of the entire NPG event. The observation heights (260 m and ground) are denoted as subscripts.

to a weak photochemical process indicated by the lowest O_3 (Figure S5). Moreover, GR_{260m}/GR_{ground} correlates well with the RH differences (RH_{260m}-RH_{ground}) under certain *T* ($20 < T < 30°C$, r = 0.92) (Figure 2B). Thus, higher RH at 260 m could be responsible for the enhanced growth aloft.

We further found that enhanced NPG at 260 m could be associated with more readily available H_2SO_4 in most cases, which has been proved to trigger the NPF events in urban Beijing, especially in the presence of stabilizing bases.[38] SO_2 at 260 m was generally higher than that at the ground, consistent with the fact that the main source of SO_2 in urban Beijing is regional transport (Figure S5D). In addition, O_3 was also higher at 260 m with $\Delta_{260\ m\text{-}ground}$ of O_3 varying from ~6 to ~26 ppb, likely suggesting stronger photochemical reactions at 260 m (Figure S5E). Although condensation sink (CS) was slightly higher at 260 m in some cases (Figure S5F), the calculated ratio of H_2SO_4 proxy between two heights ($H_2SO_{4\ 260\ m}/H_2SO_{4\ ground}$) was generally higher than 1 (Figure 3A), suggesting higher concentrations of H_2SO_4 at 260 m than at the ground. Further, we found that the larger differences of SO_2 between 260 m and ground agreed well with the higher differences of $N_{20–40}$ when SO_2 is high (SO_2 > 2ppb, r = 0.96), indicating that more particles aloft were driven by higher SO_2 concentrations under sulfur-rich conditions (Figure 3B). Taking 18 June as an example, NPG occurred with high concentrations of SO_2 (10 ppb at 260 m vs. 8 ppb at the ground level), coupled with high CS values of ~0.05 s^{-1} at both heights (Figure 3E). Thus, it was easier at 260 m to reach the point where CS can no longer suppress NPF. As a result, a high concentration of nucleation-mode particles was first detected at 260 m at 8:00 (Figure S7). During the NPG period on June 18, J_{20} at 260 m was 70% higher than that at the ground level. Consistently, $N_{20–40}$ at both heights reached a high peak around 11:00, which was 21,165 cm^{-3} at 260 m and 16,059 cm^{-3} at the ground level (Figure S8). Indeed, the size-resolved ratios between the two heights also showed a high-value region corresponding to NPG.

However, when SO_2 concentration at 260 m was low (sulfur-poor conditions), $N_{20–40}$ at 260 m was at least 20% higher than that at the ground (Figure 3B), suggesting the unknown mechanisms behind the enhanced NPG aloft. Particularly, enhanced NPG was still observed on 7 June, when the available H_2SO_4 at 260 m was much lower caused by the extremely low SO_2 concentration (Figure 3A). On 7 June, a strong wind shear appeared around 10:00, suggesting an unstable air mass (Figure 3C). Clean air mass with low PM_1 and $N_{100–550}$ dominated from 11:00. As a result, CS decreased from ~0.04 to ~0.02 s^{-1} at both heights, and NPG events were observed at both heights. In fact, an unexpected nucleation mode with a high number concentration of particles smaller than 30 nm was first detected at 260 m at 10:00 despite the relatively high concentration of pre-existing particles, indicating that NPF was not interrupted by the air mass change (Figure S7). Thus, the detected NPF could not be from horizontal transport. At that time, SO_2 (~0.2 ppb) was an order of magnitude lower than that at the ground (~1.5 ppb), suggesting much more available H_2SO_4 at the ground level, and hence cannot explain the enhanced nucleation process at 260 m. In fact, J_{20} at 260 m started to increase before 9:00, leading $J_{20\ 260m}/J_{20\ ground}$ to increase significantly from 0.9 at 9:00 to 2.2 at 11:00. Strong downdraft was observed during this period, suggesting the role of vertical transport (Figure 3C). These results suggest that the explanation could be that the NPF process occurring above the urban boundary layer was transported to the ground by the downdraft, and hence the differences of particle formation rate between 260 m and ground were not driven by the differences of H_2SO_4 concentration between the two heights.

To further showcase that NPF at the ground was associated with the downdraft, comparable NPG events occurred at both 260 m and the ground when the downdraft was strong enough. The case was observed on 10 June (Figure 3D), on which strong downdraft almost dominated the daytime period. As a result, particles associated with NPF events were detected at the same time at the two heights after 10:00. Consistently, J_{20} at the two heights were also comparable. We also found that during the NPG process, downdrafts can reduce differences between two heights by transporting particles formed at higher altitudes to the surface. When the downdraft was enhanced abruptly around 12:30 on 19 June, differences in the PNSDs between 260 m and ground level disappeared (Figure S9). Moreover, particles associated with NPG became less and then disappeared when the downdraft changed to updraft after 14:00. In addition, we analyzed the turbulence kinetic energy (TKE, calculated based on the longitudinal, lateral, and vertical components of wind) and observed that also some other NPF events can be interrupted by changes in vertical convection (Figure S10). On 17 June, the outbreak of nucleation-mode particles was observed after 10:00 a.m. at both heights, indicating the initiation process of NPF. At that time, a negative vertical wind speed was detected when the height was higher than 80 m, suggesting the descending motions within this layer. The TKE showed an overall increasing trend with

Please cite this article in press as: Du et al., Impacts of enhanced new-particle growth events above urban roughness sublayer on cloud condensation nuclei, One Earth (2024), https://doi.org/10.1016/j.oneear.2024.12.005

CellPress
OPEN ACCESS

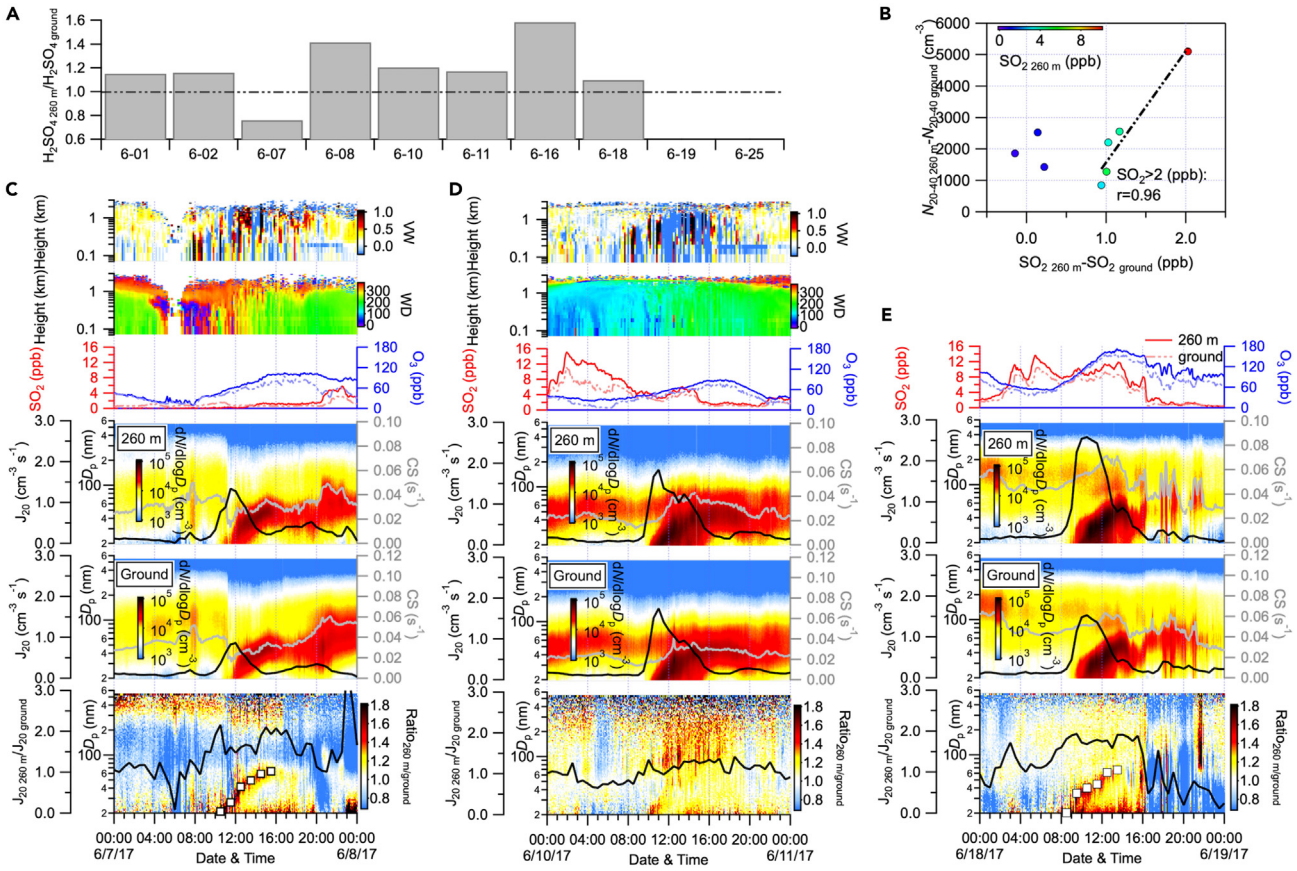

Figure 3. The role of H_2SO_4 and downdraft wind in enhanced NPG events aloft

(A) The ratios of H_2SO_4 between 260 m and ground.

(B) The scatterplot of the differences in number concentration between two heights versus those in sulfur dioxide (SO_2).

(C) One case with clear downward transport.

(D) One case with strong downward transport leading to the reduced differences of NPG events between two heights.

(E) One case with more H_2SO_4 production aloft. N_{20-40}, particle number concentration in size range from 20 to 40 nm; VW, vertical wind (negative values represent the downdraft); WD, horizontal wind direction; CS, condensation sink. O_3 is the ozone concentrations. J_{20} is the formation rate of 20-nm particles. The observation heights (260 m and ground) are denoted as subscripts. PNSDs at 260 m, at the ground, and their ratios between these two heights ($Ratio_{260m/ground}$) are also shown.

height, and TKE in the upper layer was much higher than that in the lower layer, resulting in the downward transport of the turbulence energy. However, the NPF process was interrupted when a strong updraft was observed at 14:00. Consistently, the TKE above 80 m was monotonically decreasing, suggesting that the turbulence energy was transported to the upper layer (Figure S10C). A similar case was observed on 12 June, during which the number concentration of newly formed particles decreased when a downdraft changed to an updraft after 16:00 (Figure S11). Cases with nucleation-mode particles first detected and then disappearing were also observed on 3 June at around 16:00, on 5 June at around 14:00, and on 15 June after 14:00 (Figure S12). All these results suggest that at least some of the urban NPF events in Beijing detected on the ground originated at higher altitudes. It has been found in rural environments that NPF occurring in the upper layer could be transported to the boundary layer.[27,39] The basis of this downdraft-induced NPF mechanism is that clusters formed at lower temperatures can indeed survive while being transported to warmer temperatures.[34]

During the subsequent particle growth, both H_2SO_4 and organic compounds were found to be important at the ground when SO_2 concentration was high, while organic compounds could play a dominant role under sulfur-poor conditions (Figures 3 and 4). At the ground, M_{20-100} of sulfate (SO_4) and organics (Org) at the ground showed comparably high peaks (~1.0 μg m^{-3}) on 18 June, while M_{20-100} of Org at the ground had a more pronounced high peak (~1.0 μg m^{-3}) than SO_4 (~0.2 μg m^{-3}) on 7 June. Although we did not obtain the chemical information of Aitken-mode particles at 260 m, the ratio of mass between two heights can give some indications. When the H_2SO_4 concentration was higher at 260 m, we obtained a slightly increasing of $Ratio_{260\ m/ground}$ of SO_4. As an example, $Ratio_{260\ m/ground}$ of SO_4 increased from ~0.8 to ~1.1 on 18 June, suggesting a higher contribution of SO_4 at 260 m associated with higher H_2SO_4. $Ratio_{260\ m/ground}$ of Org remained relatively constant on 18 June, while $Ratio_{260\ m/ground}$ of nitrate (NO_3) increased from ~1.7 to ~2.2 corresponding to the NPG period. However, on the sulfur-poor events, e.g., on 7 June, only

Please cite this article in press as: Du et al., Impacts of enhanced new-particle growth events above urban roughness sublayer on cloud condensation nuclei, One Earth (2024), https://doi.org/10.1016/j.oneear.2024.12.005

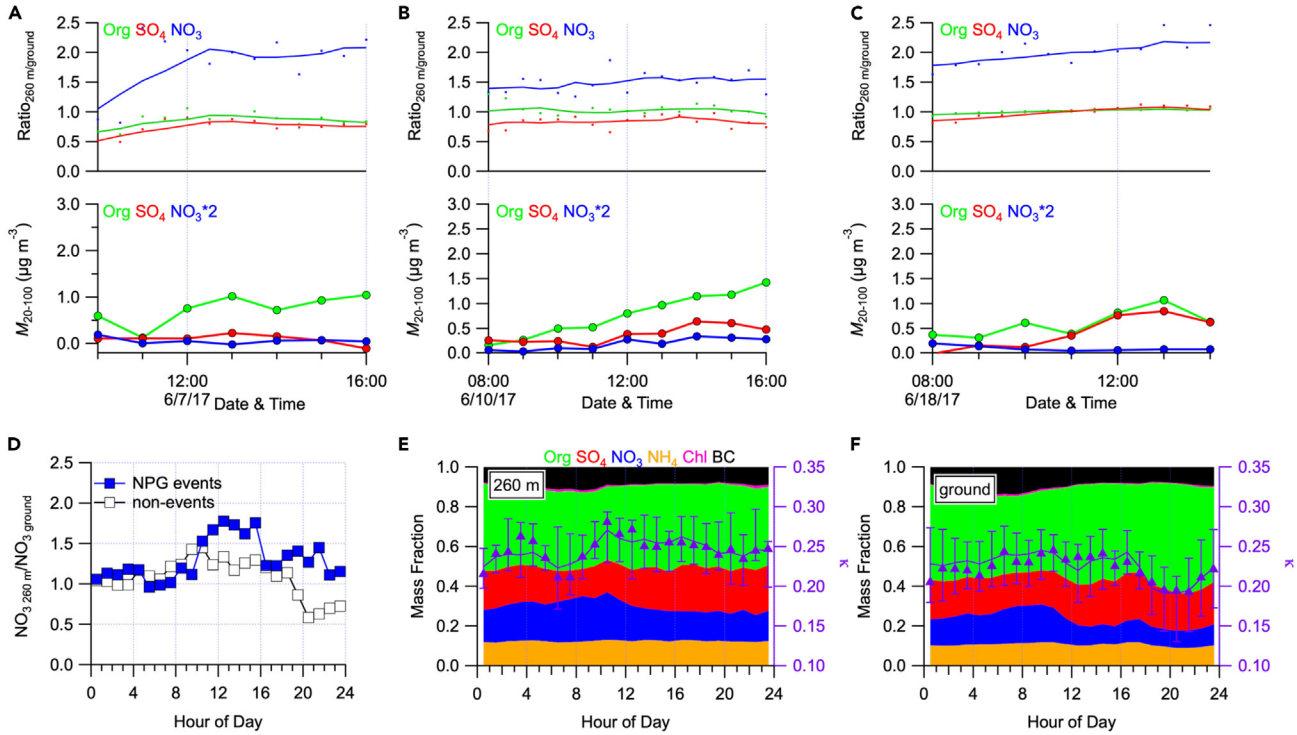

Figure 4. Chemical compositions during the particle growth process

(A–C) The evolution of chemical compositions during the growth process on 7, 10, and 18 June, respectively. The dots are raw data, and lines are six-points running average.

(D) The average diurnal variation of the ratios of nitrate between 260 m and ground on NPG-event days and non-event days.

(E and F) The mass fractions of chemical compositions and hygroscopicity parameter (κ) at 260 m and ground on NPG-event days. The 25th and 75th percentiles (bottom and top horizontal line) of κ are shown. Chemical compositions include organics (Org), sulfate (SO_4), nitrate (NO_3), ammonium (NH_4), chloride (Chl), and black carbon (BC). $M_{20–100}$ is the mass concentration in the size range from 20 to 100 nm at the ground level. $Ratio_{260m/ground}$ is the ratio of concentration between 260 m and ground.

$Ratio_{260\ m/ground}$ of NO_3 showed a more pronounced increasing trend from ~1.0 to ~2.1. These results indicated that NO_3 might play an important role during the growth process at 260 m. Moreover, on 10 June, $M_{20–100}$ of NO_3 at the ground increased from ~0.0 to ~0.2 μg m^{-3} corresponding to the NPG period, while the $Ratio_{260\ m/ground}$ kept relatively stable. This result also supported our conclusion that strong downdraft transported particles aloft to the ground, reducing differences in NPG between the two heights. On average, mass concentrations of Org and SO_4 were comparable between the two heights (Figure S13), while mass concentrations of NO_3 could be >70% higher at 260 m corresponding to the particle growth period (Figure 4D). Although $Ratio_{260\ m/ground}$ of NO_3 higher than 1 was also observed during non-event days, values were much lower. In addition, NO_3 was found to contribute more to particle mass at 260 m (17%–23%) than at the ground (9%–19%) during daytime of the NPG days (Figure 4). Recent chamber study found that nitric acid (HNO_3) and ammonia vapors can condense onto freshly nanometer particles when the temperature below about +5°C,[40] and our observation results further highlighted the possible role of NO_3 in the particle growth process larger than 20 nm above the urban roughness sublayer in summer. HNO_3 was mainly produced by the reaction between NO_2 and OH during daytime, while NO_2 was more abundant on the ground due to local traffic emissions in urban Beijing.[41] When gaseous precursors at the ground were transported to 260 m, higher RH aloft facilitated the gas-particle partitioning, which has been proved to be responsible for higher NO_3 at 260 m.[32,33] This also explained why enhanced GR highly correlated with higher RH aloft (Figure 2D). If the mixing process was suppressed, our former study found that particles at the ground would grow continuously while the particle size remained stable at 260 m, leading to a more severe haze at the ground.[20]

Impact on CCN formation

Overall, enhanced NPG at 260 m was observed in urban Beijing. It could be explained by more available H_2SO_4 at 260 m than at the ground level in most cases, while downdraft-transported NPF originating from the upper atmospheric boundary layer might also play an important role. During the subsequent growth, gaseous vapors, i.e., HNO_3, at the ground were transported to higher altitudes, where higher RH facilitated the gas-particle partitioning and hence promoted the growth. This finding, providing novel information in understanding NPF in urban Beijing, could also raise an alarm for other urban areas in that investigating NPF mechanisms without considering the influence of downdrafts has the possibility to produce misleading conclusions.

Please cite this article in press as: Du et al., Impacts of enhanced new-particle growth events above urban roughness sublayer on cloud condensation nuclei, One Earth (2024), https://doi.org/10.1016/j.oneear.2024.12.005

CellPress
OPEN ACCESS

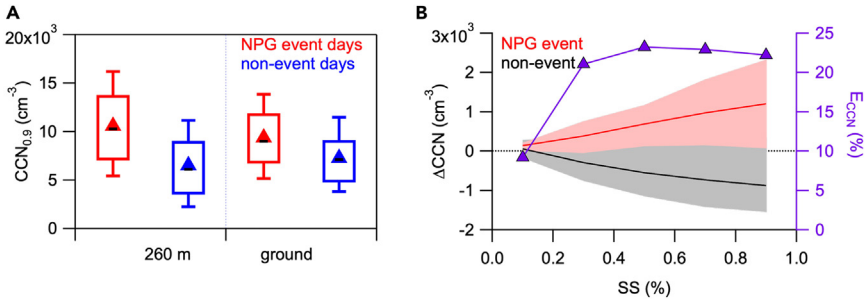

Figure 5. Impact of enhanced new-particle growth events aloft on cloud condensation nuclei

(A) The predicted CCN concentrations at 0.9% supersaturation at 260 m and ground during NPG-event and non-event days. Within each box, the median (middle horizontal line), mean (solid triangles), 25th and 75th percentiles (lower and upper box), and 10th and 90th perrcentiles (bottom and top horizontal line) are shown.

(B) The differences in CCN concentrations between two heights ($\Delta CCN = CCN_{260\ m} - CCN_{ground}$) and the changes of CCN due to enhanced NPG at 260 m (E_{CCN}). The 25th and 75th percentiles of ΔCCN during NPG event (red) and non-event (black) days are shown as shaded areas.

Further, the enhanced NPG generated more condensation nuclei (CN) at 260 m. During NPG periods, the total concentration of CN larger than 20 nm (CN_{20}) was 18,561 cm^{-3} at 260 m, which was 10% higher than the ground value of 16,828 cm^{-3} (Figure S14). On the contrary, during the daytime (8:00–16:00) of non-event days, CN_{20} at 260 m was 13% lower than that at the ground due to the higher local emissions near the ground. To further understand its climate effect, the possible impact of the enhanced NPG aloft on CCN formation was quantified. We calculated CCN concentrations by combining the PNSD and chemical composition measurements based on κ-Köhler theory (described in Methods and Note S8)[42]—a widely used method in field observations when CCN are not directly observed.[26,43–45] In general, aerosol particles can act as CCN under a given supersaturation (SS) when their size is larger than the corresponding critical size (D_{crit}), which in turn depends on the particle hygroscopicity (κ) and T. The calculated κ strongly depends on the particle chemical compositions, being higher when a particle contains more hygroscopicity species, such as NH_4NO_3. As a result of higher NO_3 contribution aloft, κ at 260 m was up to 16% higher than that at the ground during daytime. The higher κ at 260 m could contribute to a lower D_{crit}, and hence particles are more easily activated as CCN under a certain SS. For example, during NPG-event periods, CCN concentration at SS = 0.9% ($CCN_{0.9}$) was 10,562 cm^{-3} at 260 m, which was 13% higher than that at the ground value of 9,358 cm^{-3} (Figure 5A). On the contrary, during the daytime of non-event days, $CCN_{0.9}$ was 10% lower at 260 m. In fact, the differences in CCN between the two heights (ΔCCN) increased with the increasing SS. During NPG-event days, the mean ΔCCN increased from a few hundred to higher than 1,000 cm^{-3} when SS increased from 0.1% to 0.9%, while it was completely opposite during non-event days. We further investigated the enhancements of CCN from enhanced NPG at 260 m (E_{CCN}, described in Methods), and found that E_{CCN} was generally larger than 20% when SS was higher than 0.3% (Figure 5B), while E_{CCN} was ~10% when SS was 0.1%. This is because a larger D_{crit} was required for particle to be activated as CCN under a lower SS, while part of the NPG particles did not reach the D_{crit} during the selected time period. Previous *in situ* field observations already illustrated that NPF plays an important role in CCN formation, while this contribution varied between different environments.[46–49] Due to the higher particle GR associated with anthropogenic emissions, NPF-initiated enhancements in CCN number concentrations may be higher in urban environments than in remote sites.[26] Our results further suggested that CCN measurements based on *in situ* observation at the ground level might not be sufficient and the contribution from NPF might be underestimated in Beijing, and potentially in other urban areas having similar conditions. Although predicted CCN concentrations, using prescribed supersaturation, may lead to some uncertainties due to variable supersaturations of ambient clouds,[50] our analysis reduced this uncertainty by comparing the relative differences between the two heights.

While we provide novel information on understanding urban NPF and the further climate effects, several questions remain unexplained owing to the absence of long-term, continuously vertical observations within urban areas. On one hand, the instruments used in this study tracked the growth of newly formed particles instead of the initial nucleation process, making the downdraft-induced NPF not fully understood yet. On the other hand, there are some uncertainties in determining the actual climate effects of the enhanced NPF aloft in city due to the lacking CCN observations. Since Beijing represents a typical urban environment, where high values of CS are able to suppress NPF,[51,52] our results may indicate similar processes in other urban areas. Although recent studies draw attention to the vertical structure of NPF by comparing the modeled and measured results[29] in urban or mountaintop sites,[53] there are still very limited directly comprehensive vertical observations in the urban environments. Therefore, our study is important not only to understanding the climatic effect of atmospheric aerosols but also to demonstrating the urgent need for conducting comprehensive and long-term vertical observations to understand the interactions between urban NPF and boundary dynamics.

METHODS

Experimental design

The sampling site is located at the tower branch of the Institute of Atmospheric Physics (IAP), Chinese Academy of Sciences (39°58′N, 116°22′E), in Beijing, China.[20,32] A platform with various instruments at 260 m was built based on the Beijing 325-m meteorological tower to measure the chemical and physical characteristics of aerosol particles above the roughness sublayer (Figure S15; and Note S1), while another set of instruments was deployed at the ground level. To measure the chemical and physical characteristics of aerosol particles at different

heights in urban areas, two scanning mobility particle sizers (SMPS, TSI) systems equipped with the same long differential mobility analyzer (DMA, TSI, 3081A) and condensation particle counter (CPC, TSI, 3772), two seven-wavelength aethalometers (AE33, Magee Scientific), a high-resolution time-of-flight aerosol mass spectrometer (HR-ToF-AMS, Aerodyne), and an aerosol chemical speciation monitor (ACSM, Aerodyne) were deployed from 1 to 25 June, 2017 at the ground level and 260 m, respectively. To sample the dry atmospheric particles, diffusion dryers were set up in front of these instruments. In order to remove particles larger than 2.5 μm, $PM_{2.5}$ cyclones were supplied in front of these sampling lines. In addition, gaseous pollutants, including CO, SO_2, and O_3, were also recorded at both heights. Meteorological variables (e.g., wind speed [WS], wind direction [WD], RH, and temperature [*T*]) at 15 heights were also obtained from the meteorological tower observation system. In addition, a Doppler wind lidar (Windcube 200, Leosphere, Orsay, France) was deployed at the ground to obtain the wind profiles from 80 to 3,000 m. Detailed information of the sampling site and the calibration/operation of instruments is found in the Notes S3–S5) and our previous studies.[20,30,54]

Two different definitions of particle diameters were used, including mobility diameter (D_p) measured by SMPS and vacuum aerodynamic diameter (D_{va}) measured by AMS/ACSM. Assumed to be spherical particles, the ratio of D_{va} to D_p is simplified to chemically resolved particle density estimated to be 1.5 g cm^{-3} during this study.[55]

In order to evaluate the measurement uncertainties, a parallel comparison of these two SMPSs was conducted before the campaign. The two SMPSs were put side by side in the same sampling room for 2 days. The ambient air was drawn into the sampling room through a stainless-steel tube. Before sampling into the two SMPSs using the same length of sampling lines, aerosol particles were dried by diffusion silica gel dryers. Although there were slight differences within instrument uncertainties,[56] the PNSDs measured by the two SMPSs were almost the same during the comparison period. We then used a correlation analysis to check whether the differences between the two SMPSs were stable. As shown in Figure S16, we used linear fitting for the number concentrations in each size bin measured by the two SMPSs during the comparison period. The correlation coefficients (r) were higher than 0.9 in the size range from 20 to 400 nm, suggesting that the differences of these instruments are stable. In addition, the slopes of these linear fittings were consistent with the size-resolved ratios ($Ratio_{260\ m/ground}$) between the two SMPSs. Large differences with lower r were found for the measurements outside this size range, especially for particles smaller than 20 nm, due to the higher measurement uncertainty. Thus, we mainly focused on the PNSD data larger than 20 nm to ensure the data quality. Based on the correlation analysis, it is reasonable to use the size-resolved $Ratio_{260\ m/ground}$ as the correction coefficient to decrease the uncertainties when comparing the measurements obtained by the two SMPSs:

If $D_p < 30$ nm:

$$SMPS_{260processed} = SMPS_{260} / Ratio_{260\ m/ground} \quad \text{(Equation 1)}$$

If $D_p \geq 30$ nm:

$$SMPS_{groundprocessed} = SMPS_{ground} \times Ratio_{260\ m/ground} \quad \text{(Equation 2)}$$

After processing, PNSDs were in good agreement for particles larger than 20 nm, with the ratios between two SMPSs being close to 1 (Figure S17). We also calculated number concentrations in different size ranges, i.e., 20–40, 40–100, and 100–550 nm, which were used in our study. As shown in Figure S18, the timeseries of post-processed particle number concentrations in these three size ranges showed a great agreement (slope = 1, $r^2 > 0.9$) during the comparison. Specially, the value of r^2 for N_{20-40} was 0.95 and the slope was 1, suggesting that the post-processed PNSD data were reliable for further analysis. In addition, the geometric mean diameters resolved from the two SMPSs matched well after post-processing (slope = 1.0, $r^2 = 0.9$; Figure S19), slightly better than before post-processing (slope = 1.1, r^2 = 0.8). Accordingly, the calculated GR was almost the same (~5.76 nm h^{-1}) after post-processing.

Identification of NPG events

Typical NPG-event days were identified according to the following criteria: (1) outbreak of new mode particles smaller than 30 nm, and (2) continued growth of the geometric mean diameter (GMD) of new-particle mode (more than 4 h). The time when a typical banana shape appears was identified as the start time (t_{start}) of an NPG event. Further, CS (Note S6), particle GRs (Note S7), and formation rates of 20 nm particles (J_{20}; Note S8) were calculated following the methods described in Kulmala et al.[57]

H_2SO_4 proxy

Although we did not observe H_2SO_4 directly, its proxy (H_2SO_{4proxy}) can be estimated based on the solar radiation (GlobRad), SO_2, and CS measurements.[58] Thus, the ratio of H_2SO_4 between the two heights ($H_2SO_{4\ 260\ m}/H_2SO_{4\ ground}$) can be written as

$$\frac{H_2SO_{4\ 260\ m}}{H_2SO_{4\ ground}} = \frac{kGlobRad_{260\ m} SO_{2\ 260\ m}}{CS_{260\ m}} \Big/ \frac{kGlobRad_{ground} SO_{2\ ground}}{CS_{ground}} \quad \text{(Equation 3)}$$

The difference in GlobRad between these two heights should be negligible, and hence we obtain

$$\frac{H_2SO_{4\ 260m}}{H_2SO_{4\ ground}} = \frac{SO_{2\ 260\ m} CS_{ground}}{SO_{2\ ground} CS_{260\ m}} \quad \text{(Equation 4)}$$

Hygroscopicity parameter and CCN

A chemical-dependent hygroscopicity parameter (κ) was used following a simple mixing rule on the basis of chemical volume fractions.[39] All particles larger than the critical dry diameter (D_{crit}) will activate as CCN at a given supersaturation (SS). The D_{crit} can be numerically derived according to the κ-Köhler theory. Further, we predicted CCN concentration at the given SS by integrating the particle number size distribution measured by SMPS

from D_{crit} to maximum diameter (D_{max}). The detailed method can be found in Note S9.

The enhancements of CCN from enhanced NPG at 260 m is defined as

$$E_{CCN} = \frac{\Delta CCN_{NPG} - \Delta CCN_{non-event}}{CCN_{260\ m\ NPG}} \quad \text{(Equation 5)}$$

where $CCN_{260\ m\ NPG}$ is the CCN concentration at 260 m during NPG periods and ΔCCN_{NPG} and $\Delta CCN_{non\text{-}event}$ are the differences in CCN concentrations between the two heights during NPG period and non-event days, respectively.

$$\Delta CCN = CCN_{260\ m} - CCN_{ground} \quad \text{(Equation 6)}$$

RESOURCE AVAILABILITY

Lead contact

Further information and requests for resources and reagents should be directed to and will be fulfilled by the lead contact, Wei Du (wei.du@helsinki.fi).

Materials availability

This study did not generate new unique materials.

Data and code availability

Data and code are available upon request from the lead contact.

ACKNOWLEDGMENTS

This work is supported by the Strategic Priority Research Program of the Chinese Academy of Sciences (XDB0760200), National Natural Science Foundation of China (92044301), ACCC Flagship funded by the Academy of Finland (337549), and the Jenny and Antti Wihuri Foundation. Q.Z acknowledges the support from the Second Tibetan Plateau Scientific Expedition and Research (STEP) program (grant no. 2019QZKK0106).

AUTHOR CONTRIBUTIONS

W.D., J.Z., W.X., Y.W., Y.Z., Q.W., L.Z., and Y.S., performed the measurements. W.D., J.Z., W.X., Y.S., and X.C. analyzed the data. W.D. wrote the original draft. J.Z., L.D., T.V.K., J.C., R.C., Q.Z., L.Z., Z.L., F.Y., F.H., P.F., Z.W., F.B., V.-M.K., M.K., and Y.S. interpreted the results and revised the manuscript. M.K. and Y.S. supported and supervised this research.

DECLARATION OF INTERESTS

The authors declare no competing interests.

SUPPLEMENTAL INFORMATION

Supplemental information can be found online at https://doi.org/10.1016/j.oneear.2024.12.005.

Received: December 14, 2022
Revised: July 3, 2024
Accepted: December 5, 2024
Published: December 31, 2024

REFERENCES

1. Kulmala, M., Maso, M.D., Makela, J.M., Pirjola, L., Vakeva, M., Aalto, P., Miikkulainen, P., Hameri, K., and O'Dowd, C.D. (2001). On the formation, growth and composition of nucleation mode particles. Tellus Ser. B Chem. Phys. Meteorol. *53*, 479–490. https://doi.org/10.1034/j.1600-0889.2001.530411.x.
2. Kulmala, M., Petäjä, T., Ehn, M., Thornton, J., Sipilä, M., Worsnop, D.R., and Kerminen, V.M. (2014). Chemistry of atmospheric nucleation: on the recent advances on precursor characterization and atmospheric cluster composition in connection with atmospheric new particle formation. Annu. Rev. Phys. Chem. *65*, 21–37. https://doi.org/10.1146/annurev-physchem-040412-110014.
3. Venzac, H., Sellegri, K., Laj, P., Villani, P., Bonasoni, P., Marinoni, A., Cristofanelli, P., Calzolari, F., Fuzzi, S., Decesari, S., et al. (2008). High frequency new particle formation in the Himalayas. Proc. Natl. Acad. Sci. USA *105*, 15666–15671. https://doi.org/10.1073/pnas.0801355105.
4. Easter, R.C., and Peters, L.K. (1994). Binary homogeneous nucleation: temperature and relative humidity fluctuations, nonlinearity, and aspects of new particle production in the atmosphere. J. Appl. Meteorol. *33*, 775–784. https://doi.org/10.1175/1520-0450(1994)033<0775:bhntar>2.0.co;2.
5. Zhang, R., Suh, I., Zhao, J., Zhang, D., Fortner, E.C., Tie, X., Molina, L.T., and Molina, M.J. (2004). Atmospheric new particle formation enhanced by organic acids. Science *304*, 1487–1490. https://doi.org/10.1126/science.1095139.
6. Paasonen, P., Nieminen, T., Asmi, E., Manninen, H.E., Petäjä, T., Plass-Dülmer, C., Flentje, H., Birmili, W., Wiedensohler, A., Hõrrak, U., et al. (2010). On the roles of sulphuric acid and low-volatility organic vapours in the initial steps of atmospheric new particle formation. Atmos. Chem. Phys. *10*, 11223–11242. https://doi.org/10.5194/acp-10-11223-2010.
7. Kirkby, J., Duplissy, J., Sengupta, K., Frege, C., Gordon, H., Williamson, C., Heinritzi, M., Simon, M., Yan, C., Almeida, J., et al. (2016). Ion-induced nucleation of pure biogenic particles. Nature *533*, 521–526. https://doi.org/10.1038/nature17953.
8. Yao, L., Garmash, O., Bianchi, F., Zheng, J., Yan, C., Kontkanen, J., Junninen, H., Mazon, S.B., Ehn, M., Paasonen, P., et al. (2018). Atmospheric new particle formation from sulfuric acid and amines in a Chinese megacity. Science *361*, 278–281. https://doi.org/10.1126/science.aao4839.
9. Yu, F., Luo, G., Nadykto, A.B., and Herb, J. (2017). Impact of temperature dependence on the possible contribution of organics to new particle formation in the atmosphere. Atmos. Chem. Phys. *17*, 4997–5005. https://doi.org/10.5194/acp-17-4997-2017.
10. Zha, Q., Huang, W., Aliaga, D., Peräkylä, O., Heikkinen, L., Koenig, A.M., Wu, C., Enroth, J., Gramlich, Y., Cai, J., et al. (2023). Measurement report: Molecular-level investigation of atmospheric cluster ions at the tropical high-altitude research station Chacaltaya (5240 m a.s.l.) in the Bolivian Andes. Atmos. Chem. Phys. *23*, 4559–4576. https://doi.org/10.5194/acp-23-4559-2023.
11. Kulmala, M., Vehkamäki, H., Petäjä, T., Dal Maso, M., Lauri, A., Kerminen, V.M., Birmili, W., and McMurry, P.H. (2004). Formation and growth rates of ultrafine atmospheric particles: a review of observations. J. Aerosol Sci. *35*, 143–176. https://doi.org/10.1016/j.jaerosci.2003.10.003.
12. Wang, Z., Wu, Z., Yue, D., Shang, D., Guo, S., Sun, J., Ding, A., Wang, L., Jiang, J., Guo, H., et al. (2017). New particle formation in China: Current knowledge and further directions. Sci. Total Environ. *577*, 258–266. https://doi.org/10.1016/j.scitotenv.2016.10.177.
13. Kulmala, M., Petäjä, T., Mönkkönen, P., Koponen, I.K., Dal Maso, M., Aalto, P.P., Lehtinen, K.E.J., and Kerminen, V.M. (2005). On the growth of nucleation mode particles: source rates of condensable vapor in polluted and clean environments. Atmos. Chem. Phys. *5*, 409–416.
14. Chu, B., Kerminen, V.-M., Bianchi, F., Yan, C., Petäjä, T., and Kulmala, M. (2019). Atmospheric new particle formation in China. Atmos. Chem. Phys. *19*, 115–138. https://doi.org/10.5194/acp-19-115-2019.
15. Kerminen, V.-M., Chen, X., Vakkari, V., Petäjä, T., Kulmala, M., and Bianchi, F. (2018). Atmospheric new particle formation and growth: review of field observations. Environ. Res. Lett. *13*, 103003. https://doi.org/10.1088/1748-9326/aadf3c.
16. Bianchi, F., Tröstl, J., Junninen, H., Frege, C., Henne, S., Hoyle, C.R., Molteni, U., Herrmann, E., Adamov, A., Bukowiecki, N., et al. (2016). New particle formation in the free troposphere: A question of chemistry

and timing. Science *352*, 1109–1112. https://doi.org/10.1126/science.aad5456.

17. Yu, F., and Luo, G. (2009). Simulation of particle size distribution with a global aerosol model: contribution of nucleation to aerosol and CCN number concentrations. Atmos. Chem. Phys. *9*, 7691–7710. https://doi.org/10.5194/acp-9-7691-2009.
18. Zha, Q., Aliaga, D., Krejci, R., Sinclair, V.A., Wu, C., Ciarelli, G., Scholz, W., Heikkinen, L., Partoll, E., Gramlich, Y., et al. (2024). Oxidized organic molecules in the tropical free troposphere over Amazonia. Natl. Sci. Rev. *11*, nwad138. https://doi.org/10.1093/nsr/nwad138.
19. Guo, S., Hu, M., Zamora, M.L., Peng, J., Shang, D., Zheng, J., Du, Z., Wu, Z., Shao, M., Zeng, L., et al. (2014). Elucidating severe urban haze formation in China. Proc. Natl. Acad. Sci. USA *111*, 17373–17378. https://doi.org/10.1073/pnas.1419604111.
20. Du, W., Dada, L., Zhao, J., Chen, X., Daellenbach, K.R., Xie, C., Wang, W., He, Y., Cai, J., Yao, L., et al. (2021). A 3D study on the amplification of regional haze and particle growth by local emissions. npj Clim. Atmos. Sci. *4*, 4. https://doi.org/10.1038/s41612-020-00156-5.
21. Kulmala, M., Dada, L., Daellenbach, K.R., Yan, C., Stolzenburg, D., Kontkanen, J., Ezhova, E., Hakala, S., Tuovinen, S., Kokkonen, T.V., et al. (2021). Is reducing new particle formation a plausible solution to mitigate particulate air pollution in Beijing and other Chinese megacities? Faraday Discuss *226*, 334–347. https://doi.org/10.1039/D0FD00078G.
22. Bzdek, B.R., and Johnston, M.V. (2010). New Particle Formation and Growth in the Troposphere. Anal. Chem. *82*, 7871–7878. https://doi.org/10.1021/ac100856j.
23. Zhang, R., Wang, G., Guo, S., Zamora, M.L., Ying, Q., Lin, Y., Wang, W., Hu, M., and Wang, Y. (2015). Formation of urban fine particulate matter. Chem. Rev. *115*, 3803–3855. https://doi.org/10.1021/acs.chemrev.5b00067.
24. Spracklen, D.V., Carslaw, K.S., Kulmala, M., Kerminen, V.M., Mann, G.W., and Sihto, S.L. (2006). The contribution of boundary layer nucleation events to total particle concentrations on regional and global scales. Atmos. Chem. Phys. *6*, 5631–5648. https://doi.org/10.5194/acp-6-5631-2006.
25. Fanourgakis, G.S., Kanakidou, M., Nenes, A., Bauer, S.E., Bergman, T., Carslaw, K.S., Grini, A., Hamilton, D.S., Johnson, J.S., Karydis, V.A., et al. (2019). Evaluation of global simulations of aerosol particle and cloud condensation nuclei number, with implications for cloud droplet formation. Atmos. Chem. Phys. *19*, 8591–8617. https://doi.org/10.5194/acp-19-8591-2019.
26. Ren, J., Chen, L., Fan, T., Liu, J., Jiang, S., and Zhang, F. (2021). The NPF Effect on CCN Number Concentrations: A Review and Re-Evaluation of Observations From 35 Sites Worldwide. Geophys. Res. Lett. *48*, e2021GL095190. https://doi.org/10.1029/2021gl095190.
27. Lampilahti, J., Leino, K., Manninen, A., Poutanen, P., Franck, A., Peltola, M., Hietala, P., Beck, L., Dada, L., Quéléver, L., et al. (2021). Aerosol particle formation in the upper residual layer. Atmos. Chem. Phys. *21*, 7901–7915. https://doi.org/10.5194/acp-21-7901-2021.
28. Lampilahti, J., Manninen, H.E., Nieminen, T., Mirme, S., Ehn, M., Pullinen, I., Leino, K., Schobesberger, S., Kangasluoma, J., Kontkanen, J., et al. (2021). Zeppelin-led study on the onset of new particle formation in the planetary boundary layer. Atmos. Chem. Phys. *21*, 12649–12663. https://doi.org/10.5194/acp-21-12649-2021.
29. Lai, S., Hai, S., Gao, Y., Wang, Y., Sheng, L., Lupascu, A., Ding, A., Nie, W., Qi, X., Huang, X., et al. (2022). The striking effect of vertical mixing in the planetary boundary layer on new particle formation in the Yangtze River Delta. Sci. Total Environ. *829*, 154607. https://doi.org/10.1016/j.scitotenv.2022.154607.
30. Du, W., Wang, W., Liu, R., Wang, Y., Zhang, Y., Zhao, J., Dada, L., Xie, C., Wang, Q., Xu, W., et al. (2022). Insights into vertical differences of particle number size distributions in winter in Beijing, China. Sci. Total Environ. *802*, 149695. https://doi.org/10.1016/j.scitotenv.2021.149695.
31. Du, W., Zhao, J., Wang, Y., Zhang, Y., Wang, Q., Xu, W., Chen, C., Han, T., Zhang, F., Li, Z., et al. (2017). Simultaneous measurements of particle number size distributions at ground level and 260 m on a meteorological tower in urban Beijing, China. Atmos. Chem. Phys. *17*, 6797–6811. https://doi.org/10.5194/acp-17-6797-2017.
32. Sun, Y., Du, W., Wang, Q., Zhang, Q., Chen, C., Chen, Y., Chen, Z., Fu, P., Wang, Z., Gao, Z., and Worsnop, D.R. (2015). Real-Time Characterization of Aerosol Particle Composition above the Urban Canopy in Beijing: Insights into the Interactions between the Atmospheric Boundary Layer and Aerosol Chemistry. Environ. Sci. Technol. *49*, 11340–11347. https://doi.org/10.1021/acs.est.5b02373.
33. Li, Y., Du, A., Lei, L., Sun, J., Li, Z., Zhang, Z., Wang, Q., Tang, G., Song, S., Wang, Z., et al. (2022). Vertically Resolved Aerosol Chemistry in the Low Boundary Layer of Beijing in Summer. Environ. Sci. Technol. *56*, 9312–9324. https://doi.org/10.1021/acs.est.2c02861.
34. Tiszenkel, L., Stangl, C., Krasnomowitz, J., Ouyang, Q., Yu, H., Apsokardu, M.J., Johnston, M.V., and Lee, S.-H. (2019). Temperature effects on sulfuric acid aerosol nucleation and growth: initial results from the TANGENT study. Atmos. Chem. Phys. *19*, 8915–8929. https://doi.org/10.5194/acp-19-8915-2019.
35. Hamed, A., Korhonen, H., Sihto, S.-L., Joutsensaari, J., Järvinen, H., Petäjä, T., Arnold, F., Nieminen, T., Kulmala, M., Smith, J.N., et al. (2011). The role of relative humidity in continental new particle formation. J. Geophys. Res. *116*, D03202. https://doi.org/10.1029/2010jd014186.
36. Boy, M., and Kulmala, M. (2002). Nucleation events in the continental boundary layer: Influence of physical and meteorological parameters. Atmos. Chem. Phys. *2*, 1–16. https://doi.org/10.5194/acp-2-1-2002.
37. Dada, L., Chellapermal, R., Buenrostro Mazon, S., Paasonen, P., Lampilahti, J., Manninen, H.E., Junninen, H., Petäjä, T., Kerminen, V.-M., and Kulmala, M. (2018). Refined classification and characterization of atmospheric new-particle formation events using air ions. Atmos. Chem. Phys. *18*, 17883–17893. https://doi.org/10.5194/acp-18-17883-2018.
38. Yan, C., Yin, R., Lu, Y., Dada, L., Yang, D., Fu, Y., Kontkanen, J., Deng, C., Garmash, O., Ruan, J., et al. (2021). The Synergistic Role of Sulfuric Acid, Bases, and Oxidized Organics Governing New-Particle Formation in Beijing. Geophys. Res. Lett. *48*, e2020GL091944. https://doi.org/10.1029/2020gl091944.
39. Wang, J., Krejci, R., Giangrande, S., Kuang, C., Barbosa, H.M.J., Brito, J., Carbone, S., Chi, X., Comstock, J., Ditas, F., et al. (2016). Amazon boundary layer aerosol concentration sustained by vertical transport during rainfall. Nature *539*, 416–419. https://doi.org/10.1038/nature19819.
40. Wang, M., Kong, W., Marten, R., He, X.C., Chen, D., Pfeifer, J., Heitto, A., Kontkanen, J., Dada, L., Kürten, A., et al. (2020). Rapid growth of new atmospheric particles by nitric acid and ammonia condensation. Nature *581*, 184–189. https://doi.org/10.1038/s41586-020-2270-4.
41. Wang, Q., Sun, Y., Xu, W., Du, W., Zhou, L., Tang, G., Chen, C., Cheng, X., Zhao, X., Ji, D., et al. (2018). Vertically resolved characteristics of air pollution during two severe winter haze episodes in urban Beijing, China. Atmos. Chem. Phys. *18*, 2495–2509. https://doi.org/10.5194/acp-18-2495-2018.
42. Petters, M.D., and Kreidenweis, S.M. (2007). A single parameter representation of hygroscopic growth and cloud condensation nucleus activity. Atmos. Chem. Phys. *7*, 1961–1971. https://doi.org/10.5194/acp-7-1961-2007.
43. Chang, R.Y.W., Liu, P.S.K., Leaitch, W.R., and Abbatt, J.P.D. (2007). Comparison between measured and predicted CCN concentrations at Egbert, Ontario: Focus on the organic aerosol fraction at a semi-rural site. Atmos. Environ. *41*, 8172–8182. https://doi.org/10.1016/j.atmosenv.2007.06.039.
44. Saliba, G., Chen, C.L., Lewis, S., Russell, L.M., Quinn, P.K., Bates, T.S., Bell, T.G., Lawler, M.J., Saltzman, E.S., Sanchez, K.J., et al. (2020). Seasonal Differences and Variability of Concentrations, Chemical Composition, and Cloud Condensation Nuclei of Marine Aerosol Over the North Atlantic. JGR. Atmospheres *125*, e2020JD033145. https://doi.org/10.1029/2020jd033145.
45. Wang, Y., Li, Z., Zhang, Y., Du, W., Zhang, F., Tan, H., Xu, H., Fan, T., Jin, X., Fan, X., et al. (2018). Characterization of aerosol hygroscopicity, mixing

state, and CCN activity at a suburban site in the central North China Plain. Atmos. Chem. Phys. *18*, 11739–11752. https://doi.org/10.5194/acp-18-11739-2018.

46. Dameto de España, C., Wonaschütz, A., Steiner, G., Rosati, B., Demattio, A., Schuh, H., and Hitzenberger, R. (2017). Long-term quantitative field study of New Particle Formation (NPF) events as a source of Cloud Condensation Nuclei (CCN) in the urban background of Vienna. Atmos. Environ. *164*, 289–298. https://doi.org/10.1016/j.atmosenv.2017.06.001.

47. Hirshorn, N.S., Zuromski, L.M., Rapp, C., McCubbin, I., Carrillo-Cardenas, G., Yu, F., and Hallar, A.G. (2022). Seasonal significance of new particle formation impacts on cloud condensation nuclei at a mountaintop location. Atmos. Chem. Phys. *22*, 15909–15924. https://doi.org/10.5194/acp-22-15909-2022.

48. Rejano, F., Titos, G., Casquero-Vera, J.A., Lyamani, H., Andrews, E., Sheridan, P., Cazorla, A., Castillo, S., Alados-Arboledas, L., and Olmo, F.J. (2021). Activation properties of aerosol particles as cloud condensation nuclei at urban and high-altitude remote sites in southern Europe. Sci. Total Environ. *762*, 143100. https://doi.org/10.1016/j.scitotenv.2020.143100.

49. Rose, C., Sellegri, K., Moreno, I., Velarde, F., Ramonet, M., Weinhold, K., Krejci, R., Andrade, M., Wiedensohler, A., Ginot, P., and Laj, P. (2017). CCN production by new particle formation in the free troposphere. Atmos. Chem. Phys. *17*, 1529–1541. https://doi.org/10.5194/acp-17-1529-2017.

50. Kalkavouras, P., Bougiatioti, A., Kalivitis, N., Stavroulas, I., Tombrou, M., Nenes, A., and Mihalopoulos, N. (2019). Regional new particle formation as modulators of cloud condensation nuclei and cloud droplet number in the eastern Mediterranean. Atmos. Chem. Phys. *19*, 6185–6203. https://doi.org/10.5194/acp-19-6185-2019.

51. Du, W., Cai, J., Zheng, F., Yan, C., Zhou, Y., Guo, Y., Chu, B., Yao, L., Heikkinen, L.M., Fan, X., et al. (2022). Influence of Aerosol Chemical Composition on Condensation Sink Efficiency and New Particle Formation in Beijing. Environ. Sci. Technol. Lett. *9*, 375–382. https://doi.org/10.1021/acs.estlett.2c00159.

52. Cai, R., Häkkinen, E., Yan, C., Jiang, J., Kulmala, M., and Kangasluoma, J. (2022). The effectiveness of the coagulation sink of 3–10 nm atmospheric particles. Atmos. Chem. Phys. *22*, 11529–11541. https://doi.org/10.5194/acp-22-11529-2022.

53. Lai, S., Huang, X., Qi, X., Chen, L., Ren, C., Wang, Z., Wang, J., Lou, S., Chi, X., Gao, Y., et al. (2022). Vigorous New Particle Formation Above Polluted Boundary Layer in the North China Plain. Geophys. Res. Lett. *49*, e2022GL100301. https://doi.org/10.1029/2022gl100301.

54. Zhao, J., Du, W., Zhang, Y., Wang, Q., Chen, C., Xu, W., Han, T., Wang, Y., Fu, P., Wang, Z., et al. (2017). Insights into aerosol chemistry during the 2015 China Victory Day parade: results from simultaneous measurements at ground level and 260 m in Beijing. Atmos. Chem. Phys. *17*, 3215–3232. https://doi.org/10.5194/acp-17-3215-2017.

55. Salcedo, D., Onasch, T.B., Dzepina, K., Canagaratna, M.R., Zhang, Q., Huffman, J.A., Decarlo, P.F., Jayne, J.T., Mortimer, P., Worsnop, D.R., et al. (2006). Characterization of ambient aerosols in Mexico City during the MCMA-2003 campaign with Aerosol Mass Spectrometry: results from the CENICA Supersite. Atmos. Chem. Phys. *6*, 925–946.

56. Wiedensohler, A., Birmili, W., Nowak, A., Sonntag, A., Weinhold, K., Merkel, M., Wehner, B., Tuch, T., Pfeifer, S., Fiebig, M., et al. (2012). Mobility particle size spectrometers: harmonization of technical standards and data structure to facilitate high quality long-term observations of atmospheric particle number size distributions. Atmos. Meas. Tech. *5*, 657–685. https://doi.org/10.5194/amt-5-657-2012.

57. Kulmala, M., Petäjä, T., Nieminen, T., Sipilä, M., Manninen, H.E., Lehtipalo, K., Dal Maso, M., Aalto, P.P., Junninen, H., Paasonen, P., et al. (2012). Measurement of the nucleation of atmospheric aerosol particles. Nat. Protoc. *7*, 1651–1667. https://doi.org/10.1038/nprot.2012.091.

58. Dada, L., Ylivinkka, I., Baalbaki, R., Li, C., Guo, Y., Yan, C., Yao, L., Sarnela, N., Jokinen, T., Daellenbach, K.R., et al. (2020). Sources and sinks driving sulfuric acid concentrations in contrasting environments: implications on proxy calculations. Atmos. Chem. Phys. *20*, 11747–11766. https://doi.org/10.5194/acp-20-11747-2020.